View metadata, citation and similar papers at core.ac.uk
brought to you by CORE
provided by NASA Technical Reports Server

NASA-TM-111566

Rarefield-Flow Shuttle Aerodynamics Flight Model

R. C. Blanchard, K. T. Larman, C. D. Moats

Reprinted from

Journal of Spacecraft and Rockets

Volume 31, Number 4, Pages 550–556

AIAA

A publication of the
American Institute of Aeronautics and Astronautics, Inc.
370 L'Enfant Promenade, SW
Washington, DC 20024-2518

JOURNAL OF SPACECRAFT AND ROCKETS
Vol. 31, No. 4, July–August 1994

Rarefied-Flow Shuttle Aerodynamics Flight Model

Robert C. Blanchard*
NASA Langley Research Center, Hampton, Virginia 23681
and
Kevin T. Larman† and Christina D. Moats‡
Lockheed Engineering and Sciences Company, Hampton, Virginia 23666

A model of the Shuttle Orbiter rarefied-flow aerodynamic force coefficients has been derived from the ratio of flight acceleration measurements. The in-situ, low-frequency (<1 Hz), low-level ($\sim 1 \times 10^{-6}$ g) acceleration measurements are made during atmospheric re-entry. The experiment equipment designed and used for this task is the High Resolution Accelerometer Package (HiRAP), one of the sensor packages in the Orbiter Experiments Program. To date, 12 HiRAP re-entry mission data sets spanning a period of about 10 years have been processed. The HiRAP-derived aerodynamics model is described in detail. The model includes normal and axial hypersonic continuum coefficient equations as functions of angle of attack, body-flap deflection, and elevon deflection. Normal and axial free molecule flow coefficient equations as a function of angle of attack are also presented, along with flight-derived rarefied-flow transition bridging formulae. Comparisons are made between the aerodynamics model, data from the latest Orbiter Operational Aerodynamic Design Data Book, applicable computer simulations, and wind-tunnel data.

Nomenclature

a	= acceleration measurements
C	= aerodynamic force coefficient
$\overline{C}$	= normalized aerodynamic coefficient, $(C - C_c)/(C_f - C_c)$
g	= acceleration due to gravity, 9.81 m/s^2
Kn	= Knudsen number; i.e., mean-free path/12.058 m
M	= Mach number
M	= mass, kg
micro-g	= 1×10^{-6} g
S	= reference area, 249.9 m^2
V	= velocity, m/s
$\overline{V}$	= viscous parameter
X, Y, Z	= Orbiter body axis system coordinates
δ	= deflection angle, deg
α	= angle of attack, deg
ρ	= atmospheric density, kg/m^3

Subscripts

A	= axial force
bf	= body flap
c	= continuum
EL	= elevon
f	= free molecular flow
i	= the ith direction; i.e., X, Y, Z axes or normal or axial axis
N	= normal force
α	= angle of attack

Received June 14, 1993; presented as Paper 93-3441 at the AIAA 11th Applied Aerodynamics Conference, Monterey, CA, Aug. 9–11, 1993; revision received Jan. 6, 1994; accepted for publication Jan. 10, 1994. Copyright © 1994 by the American Institute of Aeronautics and Astronautics, Inc. No copyright is asserted in the United States under Title 17, U.S. Code. The U.S. Government has a royalty-free license to exercise all rights under the copyright claimed herein for Governmental purposes. All other rights are reserved by the copyright owner.

*Senior Research Engineer, Aerothermodynamics Branch, Space Systems Division, Mail Stop 366. Member AIAA.

†Senior Engineer, Space and Systems Engineering Department, 144 Research Drive. Member AIAA.

‡Engineer, Space and Systems Engineering Department, 144 Research Drive.

Introduction

THE development of a reusable space vehicle that delivers payloads to orbit in the vertical rocket configuration, and returns from orbit in a horizontal aircraft configuration, provides unprecedented opportunities to the flight research community. One unique flight research area that is assessed regularly is the aerodynamic performance of a winged re-entry vehicle traversing the rarefied-flow transition regime from free-molecule to hypersonic continuum, roughly 160–60 km in altitude. Computational fluid dynamics (CFD) research[1] was conducted during the early Orbiter development flight tests, but was not mature enough for aerodynamic design predictions. Extensive wind-tunnel testing went into the design of the Shuttle Orbiter,[2] but not under conditions for the rarefied-flow regime. There is, however, one set of data used to examine viscous effects that is shown in this report. These wind-tunnel data are taken at conditions closest to those of rarefied flow. However, prior to the initial Orbiter development flights, no applicable rarefied-flow re-entry aerodynamics test data were available.

The solution to this limitation was to adapt empirical expressions resulting from earlier flight tests of Apollo-like blunt bodies to a winged re-entry vehicle.[3] Figure 1 illustrates the status of knowledge of the rarefied-flow aerodynamics at the start of the Orbiter flight program in terms of the performance parameter lift-to-drag (L/D) and independent parameters of altitude and the rarefaction parameter Kn. The region for $10^{-3} < Kn < 10$ is the rarefied-flow transition region. This region uses an empirical formula to bridge between the hypersonic continnum ($\sim Kn < 10^{-3}$) and the free molecule flow ($\sim Kn > 10$) regimes. The region between the curves illustrates the lack of confidence in using a blunt body formula for a winged vehicle. The corresponding altitudes of the rarefied-flow transition region for the Orbiter is about 80–160 km, as shown in Fig. 1. The hatched region, for Kn less than about 10^{-3}, indicates that these flight regimes were characterized by either wind-tunnel tests, or early winged vehicle flight test programs. These programs include the X15 program and the drop test of the Shuttle Enterprise. In addition, some limited computational simulations were used to define the aerodynamics in this hatched region. At higher altitudes, corresponding to the free-molecule flow region, computational simulations were performed using a complex Shuttle geometry model composed of flat plates using diffuse surface reflection conditions and a Schaaf and Chambre formulation.[4]

Decisions were made early in the Orbiter development program to use the Orbiter as a flight test vehicle to make in-situ measurements of this largely unexplored flight regime. The High Resolution

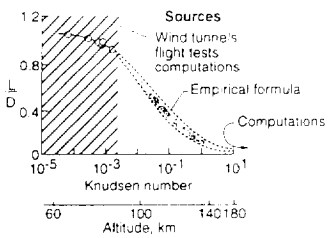

Fig. 1 Orbiter rarefied-flow aerodynamics status during early 1980s.

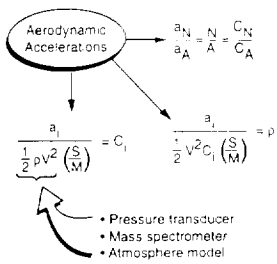

Fig. 2 Accelerometer experiment concepts.

Accelerometer Package (HiRAP) was designed and installed on the Orbiter and has been making linear acceleration measurements on the Orbiter missions since STS-6 in April 1983.[5] This capability provided flight data to construct predictive models. A rarefied-flow aerodynamic model has been formulated by examining the force coefficient ratio on multiple flights. The force coefficient ratio was used because it correlates directly to HiRAP acceleration measurement ratios.

This simple model derived from HiRAP and Inertial Measurement Unit (IMU) flight data can be used to predict both present—e.g., the Shuttle—and possibly future Shuttle-like winged re-entry vehicle rarefied-flow aerodynamics; although separate research is now available that addresses generalized bridging formulae (e.g., Ref. 6). The model incorporates aerodynamic coefficient derivative data from the OADDB[3] at the rarefied-flow transition boundaries, that is in the hypersonic continuum and in the free-molecule flow regime. In the hypersonic continuum regime, the absolute value of the individual force coefficients in the model have been adjusted to values determined on Mission STS-61C, when hypersonic continuum pressure measurements first became available. These measured pressures, converted to freestream dynamic pressures, and the measured aerodynamic accelerations were used to calculate absolute orbiter aerodynamic performance coefficients. The Orbiter control surface aerodynamic contributions, i.e., the body-flap and elevon coefficients, are generated from curve fits to the OADDB. However, to better match the average measured flight data, the elevon axial force contribution was reduced by one-third of these curve fit values for positive deflection angles. At the other end of the rarefied-flow transition boundary, the free-molecule flow force coefficient values are also generated from curve fits to the OADDB.

The purpose of this report is to present the flight measurements of the Orbiter C_N/C_A in the rarefied-flow regime for 12 missions, to provide a complete description of the flight aerodynamics model derived from these measurements, and to show the model capabilities and limitations to predict the aerodynamic force coefficients of the Orbiter in the rarefied-flow regime. To demonstrate the details, the model is used to predict the force coefficient ratios of two recent flights, STS-35 and STS-40. In addition, the model is compared with available wind-tunnel data and recent CFD calculations.

Equipment and Experiment Description

HiRAP contains three orthogonal, pendulous, gas-damped, micro-g resolution accelerometers mounted on the Orbiter in the wing box. The input axes of the accelerometer sensors are co-aligned with the Orbiter body axes. The HiRAP is designed to measure the Orbiter aerodynamic acceleration signal during re-entry. In particular, HiRAP measures the low-frequency (<1 Hz), low-level acceleration (i.e., micro-g sensitivity) signals during the re-entry from the

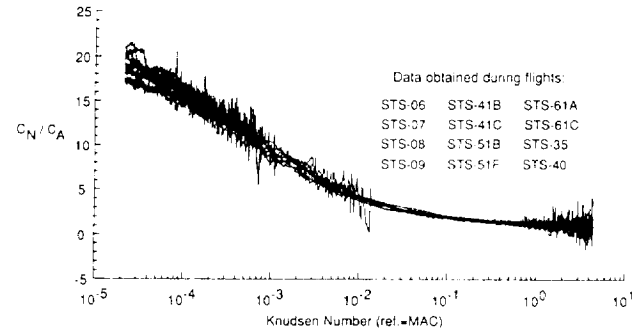

Fig. 3 HiRAP and IMU C_N/C_A flight measurements.

free-molecule flow region to the hypersonic continuum transition. During the unpowered gliding re-entry of the Orbiter, the normal-to-axial aerodynamic acceleration signal ratio is directly related to the normal-to-axial force coefficient ratio, as shown in Fig. 2.

The total acceleration signals measured by the HiRAP are converted into calibrated aerodynamic acceleration data sets and merged with mission-specific trajectory state vector data. These merged aerodynamic data sets are then further processed to determine Orbiter aerodynamic coefficients. The equation for this process, shown in Fig. 2, is a particular arrangement of the classical aerodynamic force equation:

$$C_i = \frac{a_i}{(1/2\rho V^2)S/M} \tag{1}$$

where C_i is the aerodynamic force coefficient in the ith direction, a_i is the corresponding acceleration, and S/M is the vehicle area to mass ratio. In general, the dynamic pressure $(1/2\rho V^2)$ can be obtained from air data measurements, such as pressure transducers or mass spectrometer measurements,[7] or from atmospheric models. For this report, pressure data taken in the hypersonic region of flight from STS-61C were included in the model development.[8]

To calculate the coefficient C_i in Eq. (1), all of the terms on the right of the equation must be known. The HiRAP instrument measures acceleration a_i along each Orbiter axis. The mass M and the reference area S (249.9 m^2) are known and velocity V is determined as a function of flight time from a best estimated trajectory (BET) process.[9–11] Because no measurements of the density were available for most of the earlier flights, a statistical approach was developed to determine the aerodynamic coefficient ratio using the ratio of accelerometer data. This technique is described in the literature along with the results for all of the earlier flights.[9,12–17]

Flight Data Results

The fundamental principle behind making aerodynamic acceleration measurements during re-entry is to remove the nonaerodynamic acceleration inputs. In unpowered gliding flight, the predominant nonaerodynamic forces on the Orbiter are thrust firings, auxiliary power units (APUs), and rotationally induced linear accelerations (the sensors are not at the center of gravity). The thrust firings are measured acceleration impulses induced when the reaction control system (RCS) is used to control the attitude of the Orbiter Vehicle during reentry. The three APU exhaust ports are located just in front of the vertical tail and induce a pulsing acceleration signal in the Z-axis direction. The flight data are transformed into aerodynamic acceleration data using a rigorous, detailed process reported earlier.[18,19] After this process, the ratio of aerodynamic acceleration is formed, which is also the ratio of the aerodynamic force coefficients.

A measure of aerodynamic performance is the ratio of the normal to axial acceleration measurement. This ratio corresponds to force coefficient ratios, C_N/C_A. Figure 3 presents the force coefficient ratio data during re-entry for all 12 currently available missions. The re-entry data set consists of about 11.6 hours of flight measurements. It is from this compendium of data that the aerodynamic model has been determined. For the purposes of this analysis, the acceleration data sets consist of time and X- and Z-axis acceleration

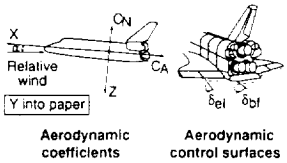

Fig. 4 Sign conventions.

measurements. The HiRAP instrument does measure and record the Y-axis sensor output, but it is not used in this paper.

Rarefied-Flow Aerodynamics Model

The analytic aerodynamics model derived from the HiRAP data has evolved over time and is documented.[9,12–17] The model has continually improved with the collection of more flight data and a better understanding of calibration factors.[18,19] This aerodynamics model is composed of curve fits to data provided in the OADDB[3] combined with a transition bridging formula developed using data from the early flights of the HiRAP instrument.[12]

The sign convention used for the model is the standard used in the Orbiter program documentation and is presented in Fig. 4. The OADDB used in the model come from the third update, which reflects the most recent normal and axial coefficient Shuttle flight information. A subset of these data were chosen that includes these parameters: angle of attack ranging from 0 to 60 deg for the payload bay doors closed (corresponding to free-molecule flow conditions), angle of attack ranging from 35 to 45 deg for the entry region, elevon deflection ranging from −15 to 22.5 deg, body-flap deflection ranging from −11.7 to 22.5 deg; viscous parameter ranging from 0.001 to 0.05, and Mach number ranging from 15 to 30. The total OADDB derived C_N and C_A aerodynamic entry coefficients were obtained by summing contributions from the basic, high-altitude, real-gas, viscous interaction, body-flap, elevator/aileron (elevon), and vehicle components. The rarefied-flow Shuttle aerodynamics flight model discussed in this paper is a simple model. It contains three segments: the hypersonic continuum, the free-molecule flow, and the transition bridging formulae. Each segment is described in detail.

Hypersonic Continuum

The formulae for the hypersonic continuum normal and axial coefficients as a function of α are as follows:

$$C_{N_{c,\alpha}} = -9.25704 \times 10^{-5}\alpha^2 + 5.23808 \times 10^{-2}\alpha - 0.839782 \quad (2)$$

$$C_{A_{c,\alpha}} = 5.86689 \times 10^{-7}\alpha^3 - 6.72027 \times 10^{-5}\alpha^2 + 3.32044 \times 10^{-3}\alpha - 0.0086314 \quad (3)$$

These equations are for the Shuttle vehicle at an angle-of-attack envelope of $35 < \alpha < 45$ deg. The coefficient functions in Eqs. (2) and (3) are resulting curve fits to the basic data in the OADDB with adjustments resulting from an earlier analysis using flight data from STS-61C.[8] Unlike the more sophisticated OADDB, the flight model basic coefficients given previously do not separate physical phenomena such as real gas and viscous effects. In effect, each equation results in one combined coefficient allowing for computation ease and, as discussed later, not introducing significant errors. Figure 5 shows the calculations using the above equations for angle of attack between 35 and 45 deg. Also included on the graphs are a comparison of the flight model force coefficients angle-of-attack behavior with the OADDB data. The conditions for the OADDB data are $M = 15$, $\bar{V} = 0.005$, and $\delta_{bf} = \delta_{EL} = 0$ deg. These conditions correspond to an altitude of approximately 58 km. Two OADDB data sets are shown; one is the OADDB basic coefficients (the circles), whereas the other (the squares) has the real gas, viscous, and vehicle effects included, i.e., a composite coefficient, comparable to the above equations. The primary difference between the individual OADDB basic coefficients and the points labeled "OADDB (total)" is real-gas effects for C_N and viscous effects for C_A. Comparing these OADDB composite coefficients with the flight model, it is seen that the flight model C_N coefficient is consistently lower by about 7% than the OADDB, while the C_A coefficient is slightly

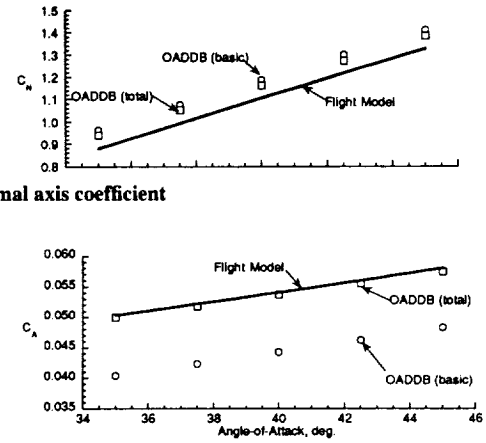

a) Normal axis coefficient

b) Axial axis coefficient

Fig. 5 Body axes coefficients comparison—hypersonic continuum.

higher (about 2%) for all angles of attack. These differences will produce noticeable differences (about 9%) in the coefficient ratio.

The Shuttle control surfaces modeled are the hypersonic continuum body flap and elevons at $\alpha = 40$ deg and $M = 20$. The normal and axial contributions for each are:

Body Flap

For $-11.7 \text{ deg} \le \delta_{bf} \le 22.5$ deg:

$$C_{N_{c,bf}} = 4.46278 \times 10^{-4} + 1.92931 \times 10^{-3}\delta_{bf} + 3.6029 \times 10^{-5}\delta_{bf}^2 \quad (4)$$

$$C_{A_{c,bf}} = 2.39178 \times 10^{-4} + 4.81862 \times 10^{-4}\delta_{bf} + 3.03937 \times 10^{-5}\delta_{bf}^2 - 3.500869 \times 10^{-7}\delta_{bf}^2 \quad (5)$$

Elevons

For $-15 \text{ deg} \le \delta_{bf} \le 15$ deg:

$$C_{N_{c,EL}} = 1.00333 \times 10^{-3} + 5.76021 \times 10^{-3}\delta_{EL} + 1.18538 \times 10^{-4}\delta_{EL}^2 \quad (6)$$

$$C_{A_{c,EL}} = 1.3981 \times 10^{-3} + 1.55864 \times 10^{-3}\delta_{EL} + 8.6081 \times 10^{-5}\delta_{EL}^2 \quad (7)$$

$$\text{if } C_{A_{c,EL}} \ge 0, \text{ then } C_{A_{c,EL}} = 1/3 C_{A_{c,EL}} \quad (8)$$

Figures 6 and 7 show the above functions compared with the data from the OADDB for the body flap and elevons, respectively. The flight model varies from the OADDB for positive elevon angles in Fig. 7 because the HiRAP flight data indicated that the elevon effectiveness was less than the OADDB predicted.

Then, the total hypersonic continuum coefficients are the following:

$$C_{N_c} = C_{N_{c,\alpha}} + C_{N_{c,bf}} + C_{N_{c,EL}} \quad (9)$$

$$C_{A_c} = C_{A_{c,\alpha}} + C_{A_{c,bf}} + C_{A_{c,EL}} \quad (10)$$

Free-Molecule Flow

The formulae for the free-molecule flow normal and axial coefficients as a function of α are:

$$C_{N_{f,\alpha}} = -7.16528 \times 10^{-6}\alpha^3 + 9.66197 \times 10^{-4}\alpha^2 + 9.18422 \times 10^{-3}\alpha + 1.58739 \times 10^{-3} \quad (11)$$

$$C_{A_{f,\alpha}} = -1.17117 \times 10^{-5}\alpha^3 + 5.92205 \times 10^{-4}\alpha^2 + 0.0164864\alpha + 0.751105 \quad (12)$$

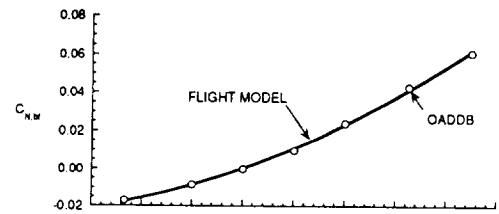

a) Normal axis coefficient increment

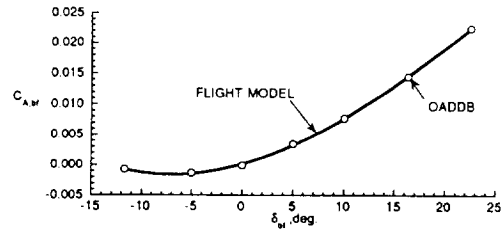

b) Axial axis coefficient increment

Fig. 6 Body-flap coefficients comparison, $\alpha = 40$ deg.

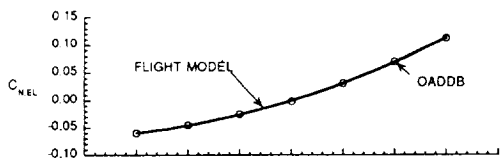

a) Normal axis coefficient increment

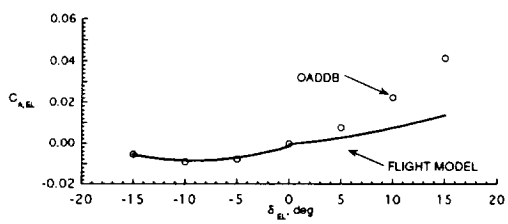

b) Axial axis coefficient increment

Fig. 7 Elevon coefficients comparison, $\alpha = 40$ deg.

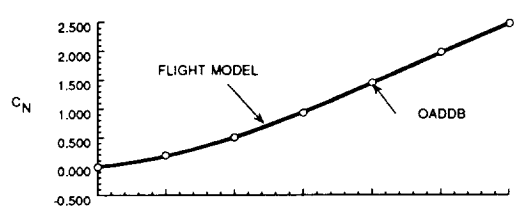

a) Normal axis coefficient

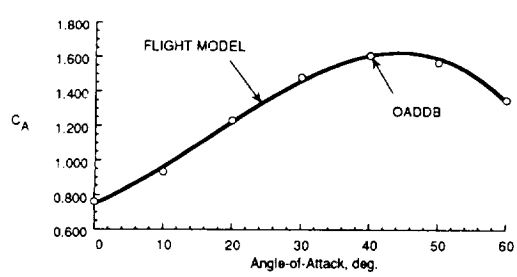

b) Axial axis coefficient

Fig. 8 Body axes coefficient comparison—free molecular flow.

Equations (11) and (12) are for the Shuttle (payload doors closed) at $0 < \alpha < 60$ deg. A comparison of these functions with the data from the OADDB is shown in Fig. 8. The body-flap and elevons contributions; that is, $C_{N_{f,bf}}$, $C_{A_{f,bf}}$, $C_{N_{f,EL}}$, and $C_{A_{f,EL}}$, in the free-molecule flow regime are undetermined and are currently set to zero.

Then, the total free-molecule flow coefficients are:

$$C_{N_f} = C_{N_{f,\alpha}} + C_{N_{f,bf}} + C_{N_{f,EL}} \tag{13}$$

$$C_{A_f} = C_{A_{f,\alpha}} + C_{A_{f,bf}} + C_{A_{f,EL}} \tag{14}$$

Bridging Formulae

The method to bridge the hypersonic continuum to the free-molecule flow regime includes the following "bridging" formulae[5,8,12,13,16]:

$$\begin{aligned} \overline{C}_N &= \exp\left[-0.29981(1.3849 - \log_{10} Kn)^{1.7128}\right] \\ &\text{if} \quad \log_{10} Kn < 1.3849 \\ &\text{otherwise} \quad \overline{C}_N = 1.0 \end{aligned} \tag{15}$$

$$\begin{aligned} \overline{C}_A &= \exp\left[-0.2262(1.2042 - \log_{10} Kn)^{1.8410}\right] \\ &\text{if} \quad \log_{10} Kn < 1.2042 \\ &\text{otherwise} \quad \overline{C}_A = 1.0 \end{aligned} \tag{16}$$

where the normalized normal and axial coefficients use Knudsen number Kn as the independent parameter. The re-entry aerodynamic coefficients are calculated by the following relationships:

$$C_N = C_{N_c} + (C_{N_f} - C_{N_c})\overline{C}_N \tag{17}$$

$$C_A = C_{A_c} + (C_{A_f} - C_{A_c})\overline{C}_A \tag{18}$$

Re-Entry Trajectory Data

Re-entry trajectory data from each mission are required for the development and the calculation of the rarefied-flow aerodynamics model. These data are available after each flight, and they represent the "as flown" trajectory.[9–11] Other information is also available, such as the as flown Orbiter configuration. The angle-of-attack and control surface data for all missions under consideration are obtained from this source and presented in Figs. 9a–9c. The Orbiter average angle of attack is seen to be 41 deg until an altitude of about 110 km is reached, when it decreases to about 40 deg. During the early Orbiter flights, the initial body-flap and elevon settings were varied, until an apparent optimum setting was realized. Currently, all flights use −4.5 and −2.7 deg as the settings for the body flap and elevons, respectively. The mass of the Orbiter at entry interface (121 km) and the velocity profile of each mission were used to complete the analysis.

Aerodynamics Model Comparisons

With Accelerometer Data

Using the above aerodynamics model and the "as flown" angle-of-attack, body-flap and elevon deflection angles, the ratio C_N/C_A can be calculated. The calculations are presented in the form of a force ratio C_N/C_A as a function of Knudsen Number Kn in Fig. 10. The Kn in this figure is derived from the 1976 *Standard Atmosphere*[20] and uses the mean aerodynamic chord of the Orbiter as a reference length (12.058 m). The ratio measurement model residuals (i.e., the difference between model predictions and the flight measurements) are also presented for all 12 missions in Fig. 10. The average residual for $Kn < 10^{-3}$ is not completely random, suggesting that further model adjustments in body-flap and/or elevon effectiveness are possible.

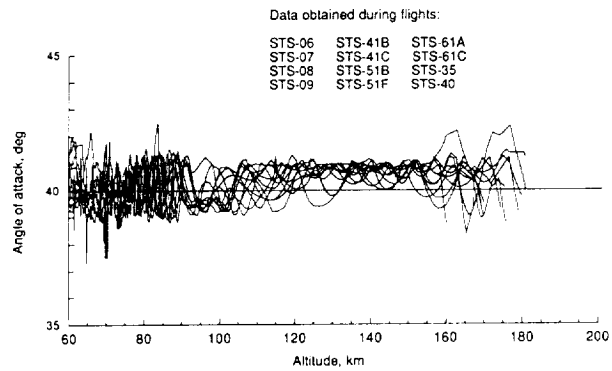

a) Orbiter angle of attack during re-entry

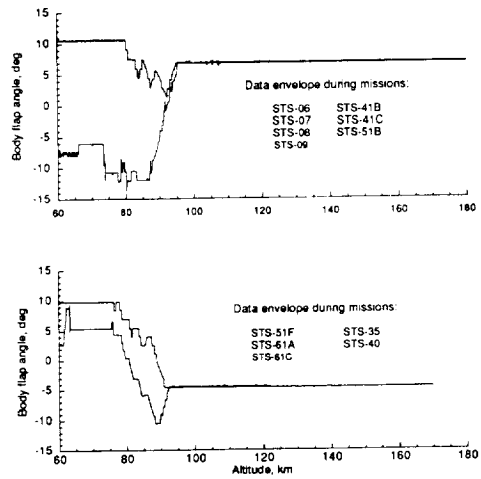

b) Body-flap deflection during re-entry

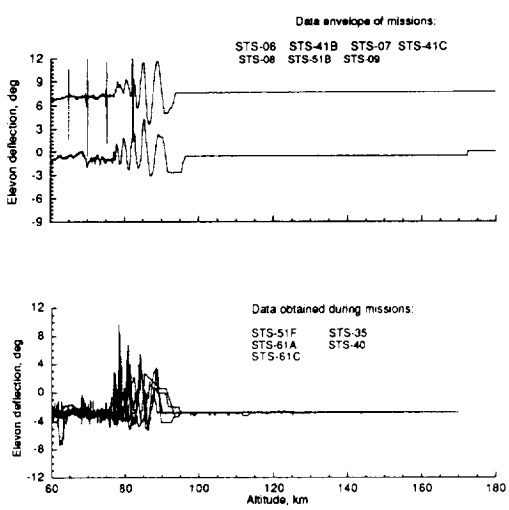

c) Elevon deflection during re-entry

Fig. 9 Angle-of-attack and control surface data.

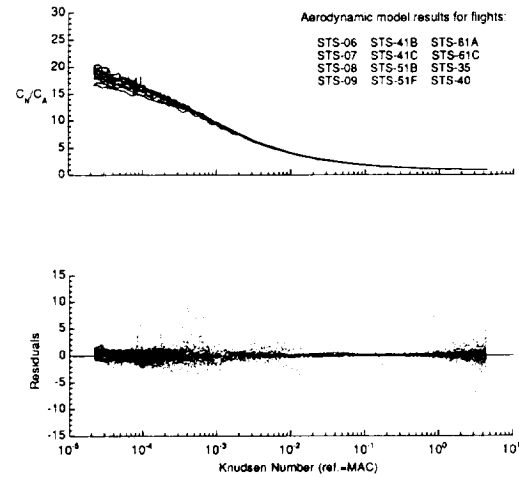

Fig. 10 C_N/C_A model results and HiRAP flight measurement comparisons.

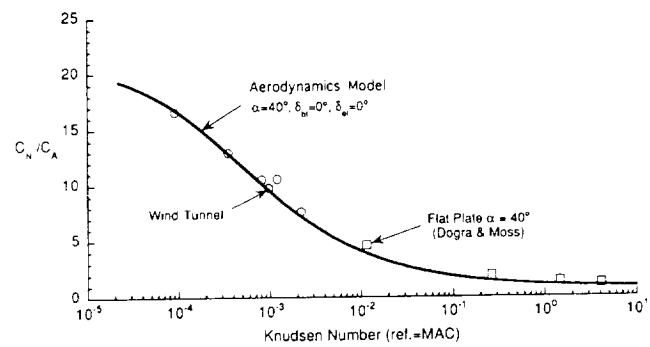

Fig. 11 Model comparison with wind-tunnel and computational data.

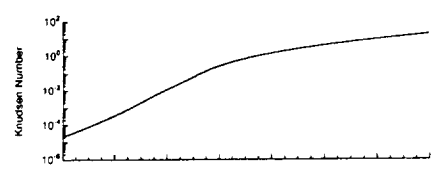

a) Kundsen number profile (1976 U.S. Standard)

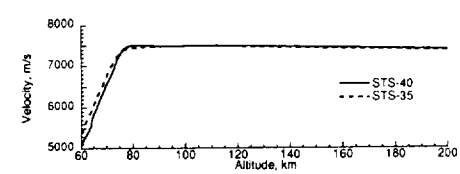

b) Velocity profiles

Fig. 12 Orbiter flight conditions.

With Other Data

Wind-tunnel data were collected by the Orbiter Project on a 1.0% scale model in a hypersonic shock-tunnel facility[2] in order to examine viscous interaction effects. The test conditions were Mach numbers up to 16 and viscous interaction parameters values up to 0.06. The data provided information on viscous interaction effects, and thus are applicable because the data are in the fringes of the rarefied-flow transition regime (i.e., up to $Kn = 0.002$). But, real-gas effects are not included in the tunnel data, and it is not a necessary condition that the tunnel data match the flight data. Shown in Fig. 11 are the C_N and C_A test results, in terms of a ratio, for $\alpha = 40$ deg and $\delta_{bf} = \delta_{EL} = 0$ deg, as a function of Kn. The HiRAP aerodynamics model agrees quite well with the wind-tunnel data in the rarefied-flow flight regime indicating that real-gas effects cancel in the ratio for this vehicle at $\alpha = 40$ deg.

Also shown in Fig. 11 is a comparison with direct simulation Monte Carlo calculations[21] performed on a flat plate of thickness and nose radius of 0.5 m and of length = 12 m, approximately the reference length of the Orbiter. The comparison with the model in the free-molecule flow regime and its fringes are excellent. All points are in good agreement with only small differences. There are several possibilities for these small differences. For example, the lower Kn points may be near the limits of the simulation, considering cell size, assumptions on number of particles simulated, etc. Or, it may simply be the difference between a three-dimensional vehicle and a flat plate simulation.

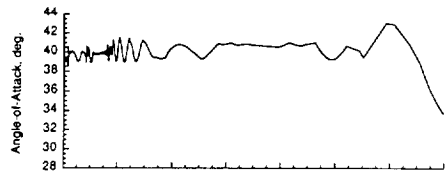

a) STS-35

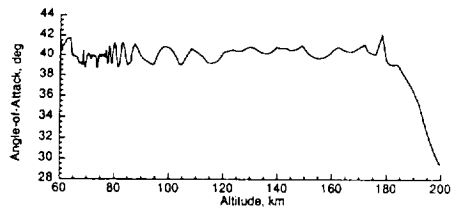

b) STS-40

Fig. 13 Orbiter angle-of-attack profiles.

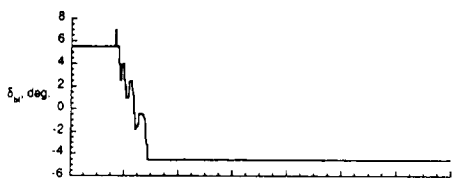

a) Body flap

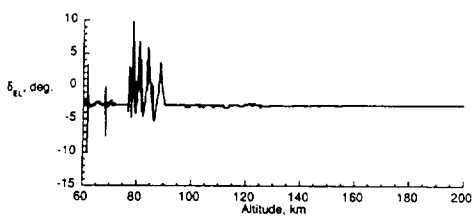

b) Elevon

Fig. 14 Orbiter control surface settings for STS-35.

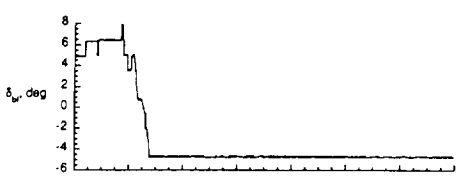

a) Body flap

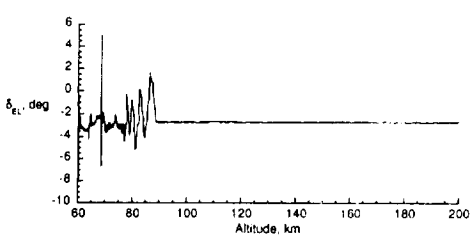

b) Elevon

Fig. 15 Orbiter control surface settings for STS-40.

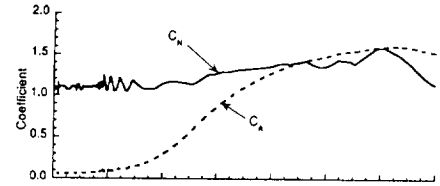

a) STS-35

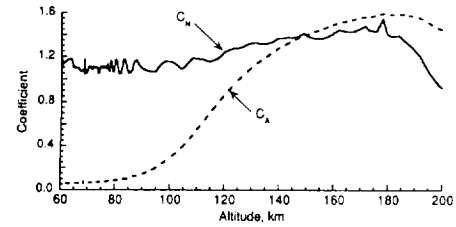

b) STS-40

Fig. 16 Flight aerodynamic model force coefficients.

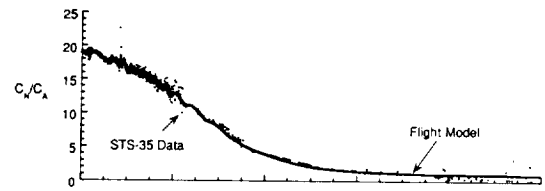

a) Flight model predictions for STS-35

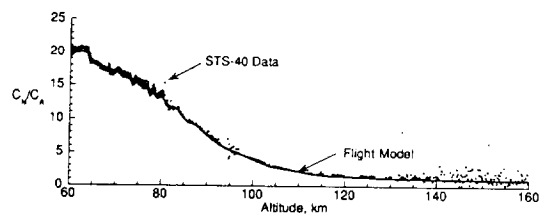

b) Flight model predictions for STS-40

Fig. 17 Comparison of predictions with STS-35 and STS-40 measured acceleration ratios.

With STS-35 and STS-40 Data

For illustrative purposes and a closer examination of the details of the model, the aerodynamics model is compared to the flight data taken on STS-35 and STS-40. The Orbiter position, velocity, and orientation information for these flights is obtained from a BET process.[10,11] This process includes using flight measurements from the inertial measurement unit (IMU) and it is the source of the IMU acceleration ratios. Figure 12 shows the Orbiter velocity and corresponding Kn as a function of altitude for STS-35 and STS-40. The Kn is computed using the 1976 U.S. Standard Atmosphere[20] using a reference length of 12.058 m, the Orbiter's mean aerodynamic chord. The Kn parameter serves as a guide as to which flow regime the vehicle resides. Namely, large Kn (roughly >10) indicate free-molecule flow behavior with few intermolecular interactions, while small Kn (roughly $<10^{-3}$) indicate near continuum flow where intermolecular collisions are an important consideration to the flow physics. Clearly, most of the altitudes included in Fig. 12 are for the rarefied-flow transition regime, where the vehicle flow is "transitioning" from free-molecule flow to continuum flow. In addition to a flow indicator, Kn is also the independent parameter for the bridging formulae presented earlier.

Figure 13 gives the angle-of-attack profile of the Orbiter vehicle for STS-35 and STS-40. Throughout the entire rarefied-flow transition into the hypersonic continuum region, about 170–60 km, the angle of attack is close to 40 deg. The corresponding control surface settings for these flights are shown in Figs. 14 and 15. Both body flap and elevon are held constant in their stored positions until shortly

below 90 km, when they are activated, mostly in the pitch direction, in order to establish longitudinal control.

An application of the STS-35 and STS-40 flight trajectory data with the rarefied-flow aerodynamics flight model described in the preceding section produces the aerodynamic performance coefficient results shown in Fig. 16. This shows the resulting angle-of-attack effects that influence both the C_A and C_N coefficients. The angle-of-attack variations are easily seen in C_N at both low and high altitudes (see Fig. 13 for comparisons). Because of scale selection, the C_A angle-of-attack variations are not easily seen at low altitudes, but are discernible at high altitudes.

Figure 17 shows two graphs, each of which contains measurements of the ratio of acceleration from the IMU and HiRAP on STS-35 and STS-40 (the IMU data are below 97 km). The differences between the model predictions and the flight data are very small, less than 1% throughout the entire regime.

Summary

The OEX program provides a unique opportunity to use the repeated Shuttle Orbiter re-entries to make in-situ aerothermodynamic and aerodynamic measurements. One of these OEX experiments, the HiRAP experiment, was developed to make low-frequency, low-acceleration aerodynamic acceleration measurements in the rarefied-flow flight transition regime. These measurements in the transition flight regime during the Shuttle Orbiter re-entry are in a flight region difficult to simulate. With the twelve HiRAP missions spanning about 10 years, a unique flight aerodynamic acceleration database has been accumulated. From this database, a concise rarefied-flow aerodynamics model has been developed. This model compares well with flight data and wind-tunnel data and recent direct simulation Monte Carlo results. This simplified aerodynamic model is useful for providing an engineering prediction of the Orbiter rarefied-flow aerodynamic performance during re-entry. In addition, it may be used as an initial engineering prediction of the aerodynamic performance of any other similar winged re-entry vehicle.

References

[1]Moss, J. N., and Bird, G. A., "Direct Simulation of Transitional Flow for Hypersonic Re-entry Conditions," AIAA Paper 84-0406, Jan. 1984.

[2]"Aerodynamics Design Substantiation Report-Vol. I: Orbiter Vehicle," Rockwell International, Space Division, Downy, CA, SD74-SH0206-1H, Jan. 1986.

[3]"Operational Aerodynamic Design Data Book," Rockwell International, Space Division, Downy, CA, STS 85-0118 CHG 3, Sept. 1991, pp. 5.2.1.1.1-9, 48, 49, 109, 148, 149, 168, 169, 188, 189, 5.2.1.1.2-9, 48, 49, 107, 146, 147, 166, 167, 186, 187.

[4]Schaaf, S. A., and Chambre, P. L., "Flow of Rarefied Gases," *Fundamentals of Gas Dynamics*, edited by Howard W. Emmons, Princeton Univ. Press, Princeton, NJ, 1958, pp. 687–738.

[5]Blanchard, R. C., and Rutherford, J. F.,"Shuttle Orbiter High Resolution Accelerometer Package Experiment: Preliminary Flight Results," *Journal of Spacecraft and Rockets*, Vol. 22, No. 4, 1985, pp. 474–480.

[6]Potter, J. L., "Procedure for Estimating Aerodynamics of Three-Dimensional Bodies in Transitional Flow," *Rarefied Gas Dynamics: Theoretical and Computational Techniques*, edited by E. P. Mintz, D. P. Weaver, and D. H. Campell, Vol. 118, Progress in Astronautics and Aeronautics, AIAA, Washington, DC, 1988, pp. 484–492.

[7]Blanchard, R. C., Duckett, R. J., and Hinson, E. W., "The Shuttle Upper Atmosphere Mass Spectrometer Experiment," *Journal of Spacecraft and Rockets*, Vol. 21, No. 2, 1984, pp. 202–208.

[8]Blanchard, R. C., Hinson, E. W., and Nicholson, J. Y., "Shuttle High Resolution Accelerometer Package Experiment Results: Atmospheric Density Measurements Between 60–160 km," *Journal of Spacecraft and Rockets*, Vol. 26, No. 3, 1989, pp. 173–180.

[9]Blanchard, R. C., Larman, K. T., and Barrett, M., "The High Resolution Accelerometer Package (HiRAP) Flight Experiment Summary for the First Ten Flights," NASA RP-1267, March 1992.

[10]Oakes, K. F., Findlay, J. T., Jasinski, R. A., and Wood, J. S., "Final STS-35 Columbia Descent BET Products and Results for LaRC OEX Investigations," NASA CR-189569, Nov. 1991.

[11]Oakes, K. F., Wood, J. S., and Findlay, J. T., "Final Report: STS-40 Descent BET Products—Development and Results," Flight Mechanics and Control, Inc., Hampton, VA, NASA CR-189570, Nov. 1991.

[12]Blanchard, R. C., and Buck, G. M., "Determination of Rarefied-Flow Aerodynamics of the Shuttle Orbiter from Flight Measurements on STS-6 and STS-7," AIAA Paper 85-0347, Jan. 1985.

[13]Buck, G. M., and Blanchard, R. C., "Rarefied Aerodynamics and Upper Atmosphere Density from Multiple Orbiter Flight Measurements," AIAA Paper 86-0269, Jan. 1986.

[14]Blanchard, R. C., "Rarefied Flow Lift-to-Drag Measurements of the Shuttle Orbiter," International Council of Aeronautical Sciences Paper 86-2.10.2, Sept. 1986.

[15]Blanchard, R. C., and Larman, K. T., "Rarefied Aerodynamics and Upper Atmosphere Flight Results from the Orbiter High Resolution Accelerometer Package Experiment," AIAA Paper 87-2366, Aug. 1987.

[16]Blanchard, R. C., and Buck, G. M., "Rarefied-Flow Aerodynamics and Thermosphere Structure from Shuttle Flight Measurements," *Journal of Spacecraft and Rockets*, Vol. 23, No. 1, 1986, pp. 18–24.

[17]Blanchard, R. C., and Hinson, E. W., "Hypersonic Rarefied-Flow Aerodynamics Inferred from Shuttle Orbiter Acceleration Measurements," International Congress on Hypersonic Aerodynamics, Paper No. 7, Sept. 1989.

[18]Thompson, J. M., Russell, J. W., and Blanchard, R. C., "Methods for Extracting Aerodynamic Accelerations from Orbiter High Resolution Accelerometer Package Flight Data," AIAA Paper 87-2365, Aug. 1987.

[19]Blanchard, R. C., Larman, K. T., and Moats, C. D., "Flight Calibration Assessment of HiRAP Accelerometer Data," AIAA Paper 93-0836, Jan. 1993.

[20]*U.S. Standard Atmosphere, 1976*, NOAA, NASA, and U.S. Air Force, Oct. 1976.

[21]Dogra, V. K., and Moss, J. N., "Hypersonic Rarefied Flow About Plates at Incidence," *AIAA Journal*, Vol. 29, No. 8, 1991, pp. 1250–1258.